Title

EQUILIBRIUM DISTRIBUTIONS OF EFFECTIVE CHARGES OF PRODUCTS OF HEAVY-ION-INDUCED SPALLATION

Author

Steiger, Naftali H.

Publication Date

1963-05-01

UCRL-10806

University of California

Ernest O. Lawrence Radiation Laboratory

EQUILIBRIUM DISTRIBUTIONS OF EFFECTIVE CHARGES OF PRODUCTS OF HEAVY-ION-INDUCED SPALLATION

DISCLAIMER

Submitted to Physical Review

UNIVERSITY OF CALIFORNIA

Lawrence Radiation Laboratory
Berkeley, California

Contract No. W-7405-eng-48

EQUILIBRIUM DISTRIBUTIONS OF EFFECTIVE CHARGES OF PRODUCTS OF HEAVY-ION-INDUCED SPALLATION

Naftali H. Steiger

May 1, 1963

EQUILIBRIUM DISTRIBUTIONS OF EFFECTIVE CHARGES OF PRODUCTS OF HEAVY-ION-INDUCED SPALLATION

Naftali H. Steiger

Lawrence Radiation Laboratory
University of California
Berkeley, California

May 1, 1963

ABSTRACT

A detailed experimental study was made of equilibrium distributions of effective charges of heavy particles of nuclear charge $Z = 66 \pm 1$ (Tb,Dy,Ho) in the velocity region 2.5×10^8 to about 6.0×10^8 cm/sec. The particles were generated by heavy-ion-induced nuclear reaction of the type (HI,xn), by bombarding various targets in the rare earth region with ions of C^{12}, N^{14}, O^{16}, F^{19}, Ne^{10}, Ne^{22}. The resultant heavy reaction products achieve charge equilibrium in the target material before leaving it. Charge-state probabilities for effective charges between 3 and 33 were found. Their distribution for a certain velocity may be approximated by a normal distribution. The mean charges obtained from these distributions fit well a linear dependence on the particle velocity. These mean charge values may, for the whole velocity region studied, be represented by Bohr's approximate theory, with the addition of a factor of two which represents the "state of condensation" effect.

Applying the results to the theory of Brunnings et al., the following γ values were obtained:

For the assumption that the electrons with smallest binding are stripped,

$\gamma = 4.9$ for $\langle v \rangle = 2.52\times10^8$ cm/sec

and $\gamma = 3.3$ for $\langle v \rangle = 5.97\times10^8$ cm/sec.

For the assumption that the outermost electrons are stripped,

$\gamma = 1.2$ for $\langle v \rangle = 2.52\times10^8$ cm/sec and

$\gamma = 0.92$ for $\langle v \rangle = 5.97\times10^8$ cm/sec.

In equilibrium the ratio of adjacent charge-state probabilities is

$$\phi_{z+1}\,\phi_z = \frac{\sigma_{loss}}{\sigma_{capture}} \propto v^{k_z} ,$$

where k_z increases very slightly with z. The magnitudes found for these ratios are in agreement with Bohr's prediction.

EQUILIBRIUM DISTRIBUTIONS OF EFFECTIVE CHARGES OF IONS IN GASES OF LOW-ION-ENERGY RADIATION*

Reftali H. Stoigert

Lawrence Radiation Laboratory
University of California
Berkeley, California

May 1, 1965

I. INTRODUCTION

Heavy particles passing through matter can lose or capture electrons in collisions with the stationary atoms of the medium traversed. This very complicated process results in the establishment of an equilibrium distribution of charges. From such a distribution the characteristic mean charge may be obtained, which relates to an element of the path of the penetrating particle; this path is long enough to include a large number of charge-exchange collisions, but too short for any appreciable slowing down of the particle.

In general the equilibrium mean charge $\langle z \rangle$ of an energetic particle when passing through matter is given by

$$\langle z \rangle = (Z_1, A_1, v, Z_2, A_2, \text{state of condensation of medium}), \qquad (1)$$

where Z_1, A_1, and v are nuclear charge, mass, and velocity of the moving particle, and Z_2 and A_2 are the nuclear charge and the mass of the atoms of the medium.

There appears to be no rigorous theory at present about the charge distribution of heavy particles as a function of the various factors shown in Eq. (1). Only for hydrogen atoms moving in a medium of atomic hydrogen has a quantum-mechanical approach been successfully used. As an example the work of Bates et al. is mentioned.[1] Other methods used are highly approximate in character, mainly based on statistical considerations, and are not in very satisfactory agreement with the experiments.[2-9] Empirical factors have therefore been introduced in order to allow

for these discrepancies. A summary of the few experimental results obtained up to 1937 and a discussion of the applicability of the existing theories have been given by Neufeld.[10]

The study of equilibrium distributions of effective charges of moving particles is of considerable theoretical as well as practical interest in a great variety of fields. Electron capture and loss phenomena constitute an important process by which low-energy heavy particles lose energy in passing through matter, and studying them may improve our still incomplete understanding of this process. Charge equilibria are also of fundamental interest in investigations of radiation damage caused by charged heavy particles, of biological effects, and of highly charged particles of cosmic origin. In recent years the importance of properties of recoiling nuclei as a source of information on nuclear reaction mechanisms has been fully recognized.[11] Knowledge of the charge distributions of the particles generated in the nuclear reactions investigated would greatly improve the interpretations of the studies. In connection with existing heavy-ion accelerators and future accelerator developments, as well as in the search for further heavy elements beyond lawrencium, the charge-distribution studies are also of considerable practical interest.

The available experimental data are mostly for particles of Z_1 up to 18 (Ar) because there have been, so far, only limited possibilities of accelerating "very heavy" ions (that is, $Z_1 > 18$). Measurements performed on fission fragments which have a continuous spread in nuclear charge, can be related only roughly to Kr and Xe, which represent the most probable nuclear charges.[12,13] Experimental studies for particles of high nuclear charge would therefore be of great interest for any further test and further development of the existing theories.

Spallation products resulting from heavy-ion-induced nuclear reactions can be produced in a wide energy interval, from a few MeV up to a few tens of MeV. Such products offer, therefore, an almost unique possibility for the study of charge equilibria of heavy particles possessing even higher Z_1 than the fission fragments.

In this report are given the results of an experimental study of equilibrium charge distributions of heavy particles of nuclear charge $Z_1 = 66 \pm 1$ (Tb,Dy,and Ho) in the velocity region from 2.5×10^8 to about 6×10^8 cm/sec. Some of the results given here have already been presented.[14]

II. EXPERIMENTAL PROCEDURE

In choosing the nuclear reactions to be utilized, the intention was to find a number of reactions which ideally would all lead to the same primary spallation product, and which should result in as wide a velocity range as possible. A number of reactions induced by heavy ions (HI) were therefore chosen, all of the type (HI,xn), most of them leading to $_{66}Dy^{149}$ as the primary spallation product. In some cases, as a compromise, for covering a certain velocity range of the resulting heavy particles reactions leading to $_{65}Tb^{149}$ as well as reactions leading to $_{67}Ho^{149}$ were also chosen. As is discussed later, this difference $\Delta Z_1 = \pm 1$ does not show any detectable influence on the results, under the experimental conditions described.

The study had to be limited to reactions for which evidence for compound-nucleus mechanism had been presented.[15,16] For these reactions the mean velocity of the spallation products can be calculated.

The heavy ions were obtained from the Berkeley heavy-ion linear accelerator (Hilac), which accelerates ions to 10.4 ± 0.2 MeV/amu.[17] Magnetic deflection was used as the charge-analyzing method. The heavy-ion beam was deflected through 30 deg by a bending magnet before reaching the deflection chamber. A schematic diagram of the magnetic deflection chamber is shown in Fig. 1. The heavy-ion beam, entering the chamber, passes through an oval-shaped opening (collimator No. 1) 5 mm high and 3 mm wide, and then penetrates an appropriate number of degrading foils.

The bombarding energy was varied, usually around the peak of the excitation function of a particular reaction, so long as the reaction cross section still

allowed reasonable reaction yields. In this way the velocity of the resulting products from a certain reaction was varied to some extent.

The energetic scattered heavy ions that emerged from the last degrading foil passed a narrow slit collimator 4 mm high and 0.7 mm wide (collimator No. 2) and hit the target after penetrating its backing material. The resulting spallation products, together with the heavy-ion beam emerging from the target, passed through an additional slit collimator (collimator No. 3) of the same dimensions as the previous one. Entering the 4-mm-high gap of a permanent magnet of 3150 gauss field strength, the charged spallation products as well as the beam ions were horizontally deflected, according to their momenta and effective charge states. The spallation products were finally collected on a thin Al catcher foil. The Faraday cup behind the catcher foil served to monitor the heavy-ion beam throughout the experiment.

The decay characteristics of the three types of primary spallation products obtained in the various cases (which are genetically related) are as follows:

$$_{67}Ho^{149} \xrightarrow[EC]{< 1\ min} {}_{66}Dy^{149} \xrightarrow[EC]{\sim 15\ min} {}_{65}Tb^{149g} \xrightarrow[0.1\ \alpha (3.95\ MeV)]{4.1\ h} \cdots$$

Therefore the counting of α tracks of the decaying Tb^{149g} obtained on a nuclear track emulsion could be used as detecting method in all the experiments. The relative horizontal distribution of the collected spallation products was recorded by taking an autoradiograph of the catcher foil on a K-2 Ilford Nuclear Track Plate for about four half-lives of Tb^{149g}. (The catcher foil was covered by a very thin plastic coating to prevent chemical reaction between the aluminum foil and the nuclear emulsion.) Finally the track plate was scanned under a microscope for α-track density as a function of horizontal distance from the beam axis.

A preliminary experiment of this type by Sikkeland seemed to be encouraging.[18] At the places on the emulsion corresponding to where the heavy-ion beam was hitting

the catcher foil, a somewhat diffuse line was obtained indicating β activity induced in the catcher foil and its plastic cover. Furthermore, long-range α tracks, which could be clearly distinguished from the short-range rare earth α tracks, were found at these places. These long-range tracks were attributed to α activity induced in heavy-element impurities existing in the catcher foil material. Test experiments following the α activity of the catcher foil, starting from the time of end of bombardment showed that after a cooling period of about 1 h, the α activity is practically governed by the 4.1-hour half-life of Tb^{149g}. However, a certain amount of long-lived long-range α activity tracks were always found on the plate at the places corresponding to where the beam hit the catcher foil. (See peaks of induced α-activity in Fig. 4.)

The position of the beam axis on the catcher foil, which corresponds to the zero-deflection position of the particles, was obtained by a short calibration run, without using a target and with no magnetic field applied. As under the experimental conditions applied--the heavy-ion beam was practically completely stripped,[19] the distance between the zero-deflection position and the position of the deflected beam was used for calibration of the charge-state scale. This deflection was determined by measuring under a microscope the distances between the induced β-activity lines on the nuclear emulsion, as well as the distances between the lines obtained directly on the catcher foil by beam-induced burn of the plastic coating.

The beam-degrading foils used were mostly commercially available rolled Al foils. The mean thickness of each foil for an area of 4 cm^2 was obtained by area and weight determinations. To prevent excessive heating of the foils, which would change their area weight or even burn them, the following precautions proved desirable:

(a) Usually only Al foils of a thickness of about 1.7 mg/cm^2 were used. When it was necessary to degrade the beam to about half energy, a number of Be foils of thickness of about 10 mg/cm^2 each were used.

(b) The beam level was kept below a certain value which, because of strong particle scattering, had to be progressively lowered as larger degrading thicknesses were used.

The beam levels used thus varied from about 10 nμA (in cases of large energy degradation) up to about 80 nμA (when no degraders had to be used).

(c) The degraders were spaced.

The targets used were thin layers of rare earth metals and $BaCl_2$[20] vacuum evaporated[21] onto thin Al or Ni backing foils. The target thickness used was usually about 100 $\mu g/cm^2$. For this target thickness, reasonable reaction yields could be obtained without causing too great a velocity spread. By using thinner targets and comparing the resultant charge distributions it could be shown that for 100 $\mu g/cm^2$ target thickness more than 90% of the spallation products leave the target after achieving charge equilibrium in it. It was found that equilibrium charge distributions were obtained, in practice, for targets thicker than 25 $\mu g/cm^2$, which corresponds to approx 10^{17} atoms/cm^2. This is of the same order as obtained by Nikolaev for heavy ions in celluloid in the same velocity region.[22]

The catcher foils used were commercially available rolled Al foils. The thickness of the foil used in a particular experiment was dependent on the velocity of the resulting spallation product. The thickness was chosen to be just enough to stop all the particles in it, but kept at a minimum so that there would be only a minimum of beam-induced radioactivity in it and so as to assure exit of the maximum number of α particles. The thicknesses used were between 0.7 mg/cm^2 and about 1.8 mg/cm^2.

Depending on the cross section for a particular reaction at a particular bombarding energy, the beam level and bombarding time were varied, so that for a large part of the experiments, the total number of spallation products caught was approximately constant. In this way the limits of statistical accuracy were about the same for the larger part of many of the experiments.

All the experiments were performed at a pressure of 10^{-4} mm Hg.

III. EXPERIMENTAL ANALYSIS

The spallation products as well as the beam particles, after entering the magnetic field, are deflected according to the well-known equation

$$H\rho = \frac{p \times c}{e \times z} \tag{2}$$

where H is the magnetic field strength, ρ the radius of curvature, c the velocity of light, p the linear momentum of the particle, e the elementary charge, and z the effective charge state of the particle.

In Fig. 2 is shown a schematic representation of the deflection geometry used. Here l is the length of the magnetic field, L the distance between the end of the magnet and the catcher foil, s the horizontal deflection of a particle by the time it reaches the end of the magnetic field, and S the additional deflection the particl has experienced when it reaches the catcher foil. On the basis of Eq. (2) and from pure geometrical considerations it can be seen that the horizontal deflection x on the catcher foil of a particle of a certain mass A_1, velocity v, and effective charge state z is given by

$$x = \frac{A_1 ev}{Hez}\left(1 - \cos \arcsin \frac{lHe}{A_1 c}\frac{z}{v}\right) + L \tan \arcsin \frac{lHe}{A_1 c}\frac{z}{v}, \tag{3}$$

where the deflection angle α appears in the form

$$\alpha = \arcsin \frac{lHe}{A_1 c}\frac{z}{v}. \tag{4}$$

The first term in Eq. (3) represents s and the second term represents S.

Figure 5 is a graphic representation of Eq. (3), giving the horizontal deflection x as a function of heavy-ion velocity v (solid line). The ratio A_1/z is the same for all the bombarding ions used (except F^{19}) and for the experimental conditions applied equals 2; l = 15.2 cm and L = 5.3 cm; H = 3150 gauss. The points scattered along the line are the mean x values obtained from the experimental determination on catcher foils and nuclear track plates, as described before in Sec. II; they fit the solid curve well. The various charge states of the deflected reaction product were thus identified by using Eq. (3), substituting for A_1 the mass of the final nuclear reaction product and for v the mean velocity of these products, $\langle v \rangle$ [see Eq. (5)].

In order to calculate the velocity of the spallation products resulting from the nuclear reactions utilized, the reaction mechanism has to be considered. The reactions utilized and the bombarding conditions applied are summarized in the first two column of Table I. Experimental investigations of the recoil properties of the final products of reactions of this type have provided a test for the validity of the statistical assumption, and have been found to favor a "compound-nucleus" reaction mechanism.[15,16,23] The excitation energies obtained in these reactions vary between about 35 and 125 MeV. At such high energies of excitation there is a very large number of overlapping levels. If we assume that in the outgoing channels the random-phase approximation still applies, the angular distribution of the evaporated neutrons should be symmetric about $\pi/2$ in the center-of-mass system. We therefore assume that an incident beam particle of lab energy E_b is absorbed to form an excited state of a compound nucleus. Because in any model for a nuclear reaction linear momentum is conserved, the momentum of the incident beam particle must be equal to the momentum of the compound nucleus. With v_{CN} denoting the velocity of the compound nucleus, which is identical with the velocity of the center-of-mass, we have

$$v_{CM}^2 = \frac{2 A_b \cdot E_b}{(A_b + A_T)^2} , \qquad (5)$$

where A_b and A_T denote the masses of bombarding particle and target atom respectively. As the compound nucleus decays, the velocities of the resulting spallation products are affected by this decay. However, when we recall that we assumed symmetric angular distribution of the evaporated neutrons, we get the result that the mean velocity (v) of the spallation products is equal to v_{CM} and is therefore given by Eq. (5).

In order to estimate the velocity spread caused by nucleon evaporation, let us consider somewhat further the decay of the compound nucleus. Let $\underset{\sim}{y}$ denote the velocity given to the spallation products in the center-of-mass system as a result of evaporation of all neutrons. Let us for further simplification assume that the neutrons are emitted in random directions in the center-of-mass system. We are then able to find an expression for the mean square value of $\underset{\sim}{y}$ for this random walk. The resulting momentum of a recoiling "mean mass" of the evaporation chain is given by

$$(A_b + A_T - \tfrac{x+1}{2} m_n)^2 \langle \underset{\sim}{v}^2 \rangle = 2 T_n m_n , \qquad (6)$$

where $(A_b + A_T - \frac{x+1}{2} m_n)$ represents the "mean mass" of the heavy product during an evaporation process of x neutrons, T_n is the average total energy removed by evaporated neutrons, and m_n is the mass of the neutron. The T_n is given by

$$T_n = E_b \frac{A_T}{A_b + A_T} + Q - T_\gamma , \qquad (7)$$

where Q is the mass difference between reactants and final products(the Q values for both the target and heavy product nuclei, have been calculated by use of Seeger's mass formula[24]),and T_γ is the average total energy of the system emitted as photons. The recoil velocity due to photon emission has been neglected. The T_n values used in the following are based on Simonoff and Alexander,[23] who measured angular distributions

of spallation products resulting from reactions similar to those given in Table I. The T_n values were obtained by assuming isotropic neutron emission.

Because of symmetric neutron evaporation $\langle \underline{v} \rangle^2$ will be zero, so that the variance of the particle will be given by $\langle \underline{v}^2 \rangle$. As is apparent from the experimental setup, a very highly collimated beam of reaction particles has been used in these experiments. Therefore, when trying to estimate the velocity spread, we need take into consideration only the velocity contributions of evaporation chains whose vector sums result in the forward and backward directions along the beam axis. Combining Eqs. (5), (6), and (7), we may estimate the velocity spread of the reaction products as a result of neutron evaporation from the expression

$$\frac{\langle v^2 \rangle}{\langle v \rangle^2} = \frac{\left(\frac{E_b A_T}{A_b + A_T} + Q - T_\gamma \right) \left(A_b + A_T \right)^2 m_n}{E_b A_b \left(A_b + A_T - \frac{x+1}{2} m_n \right)^2} . \qquad (8)$$

The velocity spread caused by target thickness was estimated from interpolation of experimental range-energy determinations of products of similar reactions in Al and Au.[15] The velocity spread caused by stopping effects in the degraders could be neglected. The geometrical spread of the reaction products has been determined experimentally for each case, and because of high collimation was found to be almost independent of scattering caused by degrader thickness.

In Fig. 4 a typical experimental scanning curve is shown, representing a track density on the nuclear emulsion plate versus deflection distance on the plate. This distance is equivalent to the horizontal deflection x of the charged reaction products obtained on the catcher foil. The scanning was performed at x values that correspond to integer values of the charge state z, for a width of ± 0.18 mm to each side of this value and for a height of 2 mm above and 2 mm below the center of the beam as defined by the slit collimator.

Two peaks of induced α activity were found. The peak corresponding to the zero-deflection position of the beam seemed not to interfere with the main curve. However, the induced α activity produced by the deflected beam was superimposed on the experimental charge-distribution curve. The curves for induced α activity for these positions were found by performing bombardments under conditions similar to those during the regular experiment, but using, instead of the target, an equivalent foil of its back material only. In this way the experimental scanning curve obtained could be corrected for the beam-induced α activity.

The curve thus obtained was corrected for velocity spread caused by neutron evaporation according to Eq. (8), for velocity spread caused by target thickness, and for geometrical spread. The resultant curve was converted into a histogram for integer values of z, representing the actual charge distribution.

Figure 5 is an example of such a histogram. This figure represents the charge distribution of Nb^{149} particles moving with a velocity of $v = 4.5 \times 10^8$ cm/sec, and was obtained from the experimental scanning curve shown in Fig. 4.

IV. RESULTS

In Table I are given a summary of the nuclear reactions utilized, the bombarding conditions, and some of the results obtained. The first column gives the nuclear reaction utilized, and the second column gives the kinetic energy E_b(lab) of the beam particles as obtained from Northcliffe's[24] range-energy curves for heavy ions. In the third column the total area weight of the beam-degrading foils, including the backing of the target layer, are given in terms of mg/cm^2 Al. The cross section given in column four is based on measurements by Alexander et al.[25] Column five gives the target thickness which is original target material, oxidized to a certain extent in $\mu g/cm^2$. Columns six and seven give nuclear charges Z_1 and Z_2, respectively, of the resultant primary spallation product and of the target medium traversed. In column eight the mean velocity, $\langle v \rangle$, of the resultant spallation product as calculated from Eq. (5) is given. In the ninth column are given the velocity spread of the spallation product caused by neutron evaporation according to Eq. (8) and caused by target thickness. The last three columns give results obtained from the corrected experimental charge distributions of the type shown in Fig. 5. Here w is the full width at half maximum of the charge distribution, z_{mp} is the most probable charge, and $\langle z \rangle$ is the mean charge of the distribution, all in positive electron units.

In Table II are presented the relative probabilities for the charge states obtained, ϕ_z (in %), as a function of various particle velocities. Only probabilities of 1% and higher are given. Each vertical column corresponds to a certain type of nuclear reaction under certain bombarding conditions, as shown in Table I. The probabilities are the mean results of a repeated number of experiments. Beside the mean velocity of the particles, $\langle v \rangle$, for each column, the nuclear charges of the moving particles (Z_1) and of the target medium traversed (Z_2) are shown.

V. DISCUSSION

A rigorous theoretical treatment of the collisions between highly charged ions and atoms is extremely complicated, and so far only very rough approximate results have been obtained. But as the approach is in most cases a statistical one, usually based on a more or less simplified Thomas-Fermi model for the electrons of the moving ion, it may be expected that these approximations should better fit measurements on ions having a high number of electrons, as in the case of fission fragments, or even still more for the present experiments, than for low-Z_1 ions.

It has been predicted by Bohr[2,4] that in the case of "very heavy" particles penetrating through a medium, the nucleus of the moving particle will along almost its whole path carry a large number of electrons which, owing to continual capture and loss, fluctuates around an average value determined by the velocity and nuclear charge of the ion and the properties of the medium. This has experimentally been verified for fission products.[12,13] These fluctuations around the average value were expected to follow a normal distribution.[8]

The experimental results obtained in this work for the different relative charge-state probabilities for various velocities (see Table II and Fig. 5) confirm that the distribution of the charges for a certain particle velocity may be approximated by a normal distribution

$$\phi_z \approx [1/\sigma(2\pi)^{1/2}] \exp [-(z-\langle z\rangle)^2/2\sigma^2] , \qquad (9)$$

where ϕ_z is the relative probability of charge state z in the distribution ($\Sigma\phi_z = 1$). This function can be characterized essentially by two parameters, the mean charge

$$\langle z\rangle = \sum_z \phi_z z \qquad (10)$$

and the distribution width

$$\sigma = \sum_{z} \phi_z (z-\langle z\rangle)^2 \quad 1/2 , \qquad (11)$$

which is related to the full width at half maximum (w) of the distribution by $w = 2.35\ \sigma$. Considering the distribution width values (w) given in Table I shows that these values increase with increasing $\langle z\rangle$ values, but the ratio $w/\langle z\rangle$ remains almost constant within the experimental error for the whole velocity region studied.

The mean charges $\langle z\rangle$ given in the last column of Table I were calculated by Eq. (10). The differences obtained between $\langle z\rangle$ and the most probable charge z_{mp} given in column 12 of Table I are within the experimental accuracy, and all the distributions obtained may therefore be considered as practically symmetrical.

In Fig. 6 a plot of the mean charge $\langle z\rangle$ as a function of particle mean velocity $\langle v\rangle$ is given. It can be seen that in the velocity region studied the experimental points fit well, within the experimental error, a linear change of $\langle z\rangle$ with $\langle v\rangle$.

Beside each experimental point the nuclear charge Z_1 of the moving reaction product is given. As may be seen from the results, no influence because of $\Delta Z_1 = \pm 1$ could be found within the experimental limits. The point for the lowest velocity measured ($\langle v\rangle = 2.52 \times 10^8$ cm/sec), which is for $Z_1 = 65$ (Tb), fits well the extrapolated line obtained for higher velocity values of $Z_1 = 66$ (Dy). The same applies for $Z_1 = 67$ (Ho), where resultant $\langle z\rangle$ values for two different velocities are shown. A more detailed comparison can be made for the results obtained for velocity $\langle v\rangle = 4.24 \times 10^8$ cm/sec. For this velocity the charge-state distribution of Ho^{149} particles as well as of Dy^{149} particles obtained by two different nuclear reactions has been studied in detail. It can be seen from Table II that the charge-state probabilities obtained for these two cases are practically identical within the experimental error. The difference in binding energy of the electrons involved, calculated for the whole charge distribution, is estimated as about 3%, which is less than the actual experimental error. Therefore no significant influence in the results because of differences $Z_1 = \pm 1$ could even be expected.

In Fig. 7, as an example, the probabilities for charge states 5, 10, 15, 20, and 25 as given in Table II are plotted as a function of particle velocity; smooth curves were obtained.

We will now try to consider the results obtained on the basis of Bohr's theory on the stopping of fission fragments.[2,4,7] This theory is based on an assumption that a heavy particle of large nuclear charge Z_1, when passing through a medium, is stripped of all its orbital electrons that have velocities less than the translational velocity of the particle. It is expected that probabilities for capture and loss of electrons by the moving ionized particle become equal when the ratio of electronic to ionic velocities is of the order of unity. Bohr uses for the description of the ion constitution a simplified statistical model of the Thomas-Fermi atom, obtaining an approximate expression for the velocity distribution of the larger part of the electrons bound in the ground state of a heavy ion of effective charge $\langle z \rangle$ corresponding to a considerable fraction of the nuclear charge. If we substitute the velocity of the moving heavy particle for the velocity of the most loosely bound electron in the ground stat of the ion, a rough estimate of the ionic mean charge we obtain

$$\langle z \rangle = Z_1^{1/3} v \Big/ (e^2/\hbar) \qquad (12)$$

applying to particle velocities in the region $e^2/\hbar < v < Z_1^{2/3} v_o$. Here $e^2/\hbar$ represents the velocity of the electron in the ground state of the hydrogen atom; $Z_1^{1/3}$ stands for the "effective quantum number" ν of the binding state. According to Bohr and Lindhard this broad maximum value for the effective quantum number applies in first approximation to a relatively large number of orbital electrons.[8] Still, since the maximum value of ν is not reached until the number of electrons retained exceeds half the nuclear charge, it is essential for the applicability of Eq. (12) that $\langle z \rangle$ be somewhat smaller than $Z_1/2$.

It is a well-established experimental fact that ions passing through a liquid or solid possess higher mean charges than ions of the same velocity passing through a gas. This "state of condensation" effect depends, according to Bohr and Lindhard,[8] upon the relative values of the time necessary for more uniform distribution of the energy of a few lightly excited electrons, τ_{dis}, and the time elapsing between two collisions, τ_{col}. For solids and liquids $\tau_{col} < \tau_{dis}$. The competition between collisions and distribution of energy between ion electrons may thus allow the excitation of the ion to exceed the minimum energy for ionization. According to Neufeld and Snyder[27] the state-of-condensation effect for heavy ions may be due to two factors: One is the "close collisions" effect which may be explained as pointed out by Lindhard and Bohr, and the other is the "distant collisions" effect which is due to the reaction of the medium that causes autoionization.

In order to be able to apply Eq. (12), which is based on a model of an atom in the ground state, to a condensed medium, one must know the distribution of electronic orbital velocities in an ion that is continually perturbed by collisions at high frequency. As this distribution is unknown, Bohr and Lindhard,[8] on the basis of qualitative considerations and Lassen's experimental results,[12] introduced into Eq. (12) for fission fragments a semi-empirical factor of 3/2.

There are so few experimental data for $\langle z \rangle$ values for "very heavy" particles in solid media that it is impossible to make any intelligent comparison with the estimates obtained by calculating from Eq. (12) and applying the factor 3/2 for solid media.

In Table III are given experimental results and theoretical estimates for some "very heavy" ions for velocities of the order of 6×10^8 cm/sec.

As no measurements in solids in this velocity domain have been performed for light fission fragments results for $v = 11 \times 10^8$ cm/sec are given.

It can be seen that, as predicted by Bohr,[7] Eq. (12) yields reasonable results for heavy fission fragments in this velocity domain, where the use of the value $Z_1^{1/3}$ for the effective quantum number seems to be justified, whereas its use for

particles of lower Z_1 shown to be inadequate.

We have not performed any charge measurements in a low-pressure gas phase for particles of $Z_1 = 66$. We assume that for the highest velocity measured--that is, $\langle v \rangle = 5.97 \times 10^8$ cm/sec for which the highest degree of ionization has been obtained--the condition given by Bohr and Lindhard for the applicability of $Z_1^{1/3}$ as the effective quantum number is still fulfilled. Equation (12) thus provides us an estimate of $\langle z \rangle$ for particles of nuclear charge = 66 in a low-pressure gas phase, which would be $\langle z \rangle = 11$. Comparing this gaseous-state with our experimental results for solid media, results in an increased empirical factor of about 2. This increased factor may be attributed to the higher Z_1 of the particles than in the case of heavy fission fragments. This also fits the experimental observation that the excess of ionization, as a result of the state-of-condensation effect of a certain velocity, has been observed to increase with the nuclear charge of the ion.[22] However, because of lack of additional experimental data for the gas and solid phase for particles of equal velocity but increasing Z_1, no regularity could be found in the excess of ionization as a result of the state-of-condensation effect.

A theoretical estimate of $\langle z \rangle$ given by Brunnings, Knipp, and Teller[5,6] is based on a more detailed Thomas-Fermi statistical model for the electrons of the ion. They assumed, as did Bohr, that the characteristic velocity of the electron v_o is roughly proportional to the particle velocity, but introduced an empirical factor of proportionality, γ, putting $v_o = \gamma v$. The characteristic velocity of the electron was calculated for two different assumptions: (a) that the characteristic velocity is equal to the root-mean-square velocity of the energetically most easily removable electron; (b) that the characteristic velocity is equal to the root-mean-square velocity of the outermost electron.

In Fig. 8 the corresponding curves calculated for an ion of $Z_1 = 66$ are shown, (Curves (a) and (b)). The dashed line (curve c) is according to Bohr's theory

for heavy fission fragments (Eq. (12)). The straight full line (curve d) shows our experimental results, assuming $\gamma = 1$. The following γ values were obtained.

For assumption (a),

$\gamma = 4.9$ for $\langle v \rangle = 2.52 \times 10^8$ cm/sec, decreasing to

$\gamma = 3.3$ for $\langle v \rangle = 5.97 \times 10^8$ cm/sec.

Applying assumption (b), we see that for the whole velocity range measured, γ is close to unity, being

$\gamma = 1.2$ for $\langle v \rangle = 2.52 \times 10^8$ cm/sec, and

$\gamma = 0.92$ for $\langle v \rangle = 5.97 \times 10^8$ cm/sec.

Even our experimental results fit fairly well the curve based on assumption (b), it must be remembered that the approach of Brunings et al. is for an ion in the ground state and therefore cannot directly apply to measurements in solids. The γ values obtained have to be considered as empirical ones, containing the ratios between what is assumed to be the characteristic velocity of the electron and the velocity of the ion, as well as the effect of the state of condensation. It can also be seen from Fig. 8 that the factor of about 2 obtained when applying Eq. (12) holds for the whole velocity region studied by us.

Values of electron capture and loss cross sections cannot be determined without a measurement for a nonequilibrium state, which in this work seemed not to be possible because of experimental reasons. However, it is possible to determine the ratio of loss to capture cross sections for a particular electron from the equilibrium relations.

If the possibility of events in which two electrons are transferred in a single collision is neglected,[23] and with the condition $\Sigma \phi_z = 1$, we find that at equilibrium the ratio of adjacent charge-state probabilities ϕ_{z+1}/ϕ_z is equal to the ratio of the electron-loss cross sections to the electron-capture cross sections for the $(z+1)$th electron:

$$\frac{\phi_{z+1}}{\phi_z} = \frac{\sigma_{z,z+1}}{\sigma_{z+1,z}} = \frac{\sigma_{loss}}{\sigma_{capture}} . \qquad (13)$$

These ratios are given in Table IV for charge states between 5 and 30. In Fig. 9 some of these ratios (for z = 6, 12, 18) as a function of particle velocity (v) are shown.

Based on the ratios obtained, and within the experimental error limits, it can be seen that

$$\frac{\phi_{z+1}}{\phi_z} \propto v^{k_z} , \qquad (14)$$

where k_z increases very slightly with z. Bohr estimated that for heavy fission fragments penetrating through heavy stopping materials, σ_l and σ_c should be of the same order of magnitude, so that the ratios are expected to be of the order of one;[7] the results presented here are in confirmation of this estimate.

In Fig. 10 the experimental results obtained for the mean charge (z) are shown as a function of $v^{1/2}$, together with the few existing measurements performed for "very heavy" ions in solids. The abscissa of $v^{1/2}$ was chosen following Lassen's suggestion for a linear relationship between the mean charge of a fission product and $v^{1/2}$ in this velocity region.[30,31] It may be seen that, as well as representing our experimental data for (z) by a linear relationship with (v) (see Fig. 7), we can also represent them fairly well as even a linear function of $v^{1/2}$. It can be seen that Lassen's results for light fission fragments[12] extrapolated to light stopping materials, together with data from Almqvist et al. for bromine ions of lower velocity,[32] fit quite well a linear dependence on $v^{1/2}$. Because there are almost no experimental data for charge distributions of "very heavy" particles, it it impossible at this stage to find even any empirical regularity for the mean charge of such a particle as a function of its velocity and nuclear charge. Additional experimental data for "very heavy" particles of various nuclear charges at various

velocities are required before any phenomenological analysis of the results and a closer examination of the existing approximate theories are possible.

VI. ACKNOWLEDGMENTS

The author wishes to thank Dr. Torbjörn Sikkeland and Dr. John M. Alexander for many helpful discussions concerning this work. He is greatly indebted to Dr. Albert Ghiorso for encouraging interest during all the phases of this work. He would like to acknowledge the assistance of the Hilac crew for many hours of operating time, and to express thanks to Charles A. Corum for the design of some of the experimental components. David G. O'Connell was most helpful in preparing some of the targets used in the experiments. The author thanks Professor Isadore Perlman for the pleasant hospitality of the Nuclear Chemistry Division of the Lawrence Radiation Laboratory.

This work was done under the auspices of the U. S. Atomic Energy Commission.

FOOTNOTES AND REFERENCES

*Work done under the auspices of the U. S. Atomic Energy Commission.

†On leave of absence from the Israel Institute of Technology, Haifa, Israel.

1. D. R. Bates and G. W. Griffing, Proc. Phys. Soc. (London) A60, 90 (1955).
2. N. Bohr, Phys. Rev. 58, 654 (1940).
3. W. E. Lamb, Phys. Rev. 58, 696 (1940).
4. N. Bohr, Phys. Rev. 59, 270 (1941).
5. T. Knipp and E. Teller, Phys. Rev. 59, 659 (1941).
6. G. H. N. Drummings, T. Knipp, and E. Teller, Phys. Rev. 60, 657 (1941).
7. N. Bohr, Kgl. Danske Videnskab. Selskab. Mat.-Fys. Medd. 18, No. 8 (1948).
8. N. Bohr and T. Lindhard, Kgl. Danske Videnskab. Selskab. Mat.-Fys. Medd. 28, No. 7 (1954).
9. I. S. Dmitriev, Soviet Physics JETP 5, 473 (1957).
10. G. Neufeld, On the Relationship Between the Charge of an Ion and Its Velcity, Oak Ridge National Laboratory Report ORNO-2365 and 2365 Supplement, Oct. 1957.
11. B. G. Harvey, Ann. Rev. Nucl. Sci. 10, 235 (1960).
12. N. O. Lassen, Kgl. Danske Videnskab. Selskab. Mat.-Fys. Medd. 30, No. 8 (1955).
13. C. B. Fulmer and B. C. Cohen, Phys. Rev. 109, 94 (1958).
14. Naftali H. Steiger, Proceedings of the Third Conference on Reactions Between Complex Nuclei, Asilomar, California, April 1963. (University of California Press, Berkeley 1963) in press.
15. L. Winsberg and J. M. Alexander, Phys Rev. 121, 518 and 529 (1961).
16. J. M. Alexander and D. H. Simon, Recoil Range Evidence for the Compound-Nucleus Mechanism in Reactions Between Complex Nuclei, Lawrence Radiation Laboratory Report UCRL-10093, April 1962.
17. E. L. Hubert et al. Rev. Sci Instr. 32, 621 (1961).
18. T. Sikkeland, (Lawrence Radiation Laboratory), private communication.
19. H. H. Heckman, E. L. Hubbard, and W. B. Simon, Electronic Charge Distributions for Heavy Ions of High Velocities, Lawrence Radiation Laboratory Report UCRL-10269 May 1962.

20. As Nd^{142} targets, an enriched isotope of 97.4% isotopic purity was used. As Ba^{138} targets, $BaCl_2$ of enriched isotopic purity of 98.0% was used. The separated isotopes were obtained from the Division of Isotopes of the Oak Ridge National Laboratory.

21. The evaporations were performed by Daniel G. O'Connell of this Laboratory.

22. V. S. Nikolaev, I. S. Dmitriev, L. N. Fateeva, and Ya. A. Teplova, Soviet Physics JETP 12, 627 (1961).

23. G. N. Simonoff and J. M. Alexander, Angular Momentum Effects on Neutron Emission by Dy and Tb Compound Nuclei, Lawrence Radiation Laboratory Report UCRL-10099-Rev. Sept. 1962.

24. P. A. Seeger, Nucl. Phys. 25, 1 (1961).

25. L. C. Northcliffe, Phys. Rev. 120, 1744 (1960).

26. J. M. Alexander and G. N. Simonoff, Excitation Functions for Tb^{149} from Reactions Between Complex Nuclei, Lawrence Radiation Laboratory Report UCRL-10525, Oct. 1962; also private communication.

27. T. Neufeld and W. S. Snyder, Phys. Rev. 107, 96 (1957).

28. Capture of several electrons in a single encounter has been observed recently by Nikolaev et al. (reference 29).

29. V. S. Nikolaev, L. N. Fateeva, I. S. Dmitriev, and Ya. A. Teplova, Soviet Physics JETP 16, 67 (1962).

30. N. O. Lassen, Phys. Rev. 69, 137 (1946).

31. N. O. Lassen, Kgl. Danske Videnskab. Selskab. Mat.-Fys. Medd. 25, No. 11 (1949).

32. E. Almqvist, C. Broude, M. A. Clark, J. A. Kuehner, and A. E. Litherland, Can. J. Phys. 40, 954 (1962).

Table I. Summary of experimental conditions and some results in charge distribution studies (symbols as used in text).

Nuclear reaction	E_b (lab) (MeV)	Degrader thickness (mg/cm^2 Al)	σ (mb)	Target thickness ($\mu g/cm^2$)	Z_1	Z_2	$\langle v \rangle \times 10^{-8}$ (cm/sec)	Velocity spread (%) caused by: Neutron evaporation	Velocity spread (%) caused by: Target thickness	w	z_{mp}	$\bar{z}$
										(positive electron units)		
$Pr^{141}(C^{12},4n)Tb^{149}$	64.0	1.7 backing / 36.0 Be degr.	35	103	65	59	2.52	9.3	3.2	7±1	9±1	9.7±0.4
$Nd^{142}(C^{12},5n)Dy^{149}$	95.2	22.8	440	115	66	60	3.05	11.1	2.9	9±1	11±1	12.4±0.4
$Nd^{142}(C^{12},5n)Dy^{149}$	112.0	10.5	170	115	66	60	3.30	12.2	2.7	9±1	12±1	12.9±0.4
$Pr^{141}(N^{14},6n)Dy^{149}$	105.7	19.9	295	103	66	59	3.45	10.9	2.6	9±1	12±1	13.6±0.4
$Ce^{138}(O^{16},7n)Dy^{149}$	133.1	14.7	270	73	66	58	4.08	10.0	1.5	10±1	15±1	15.2±0.5
$Ce^{138}(O^{16},7n)Dy^{149}$	141.0	11.6	262	73	66	58	4.24	10.8	1.4	10±1	16±1	16.0±0.5
$Pr^{141}(O^{16},8n)Ho^{149}$	144.5	10.1	180	103	67	59	4.24	10.3	1.8	10±1	16±1	16.1±0.5
$Pr^{141}(O^{16},8n)Ho^{149}$	162.0	2.1	200	103	67	59	4.50	10.6	1.7	11±1	17±1	17.6±0.5
$La^{139}(F^{19},9n)Dy^{149}$	166.2	11.4	150	127	66	57	4.64	10.0	2.2	11±1	18±1	18.1±0.4
$Ba^{138}(Ne^{20},9n)Dy^{149}$	181.6	8.1	135	124	66	56	5.27	10.0	1.9	11±1	21±1	20.8±0.8
$Ba^{138}(Ne^{22},11n)Dy^{149}$	215.0	4.3	90	124	66	56	5.97	9.9	1.7	13±1	22±1	23.3±0.9

UCRL-10806

Table II. The relative probabilites of the different charge states ϕ_z (%) for various particle velocities (symbols as used in text).

Z_1	65	66	66	66	66	66	67	67	66	66	66
Z_2	59	60	60	59	58	58	59	59	57	56	56
$\langle v \rangle \times 10^{-8}$	2.52	3.05	3.30	3.45	4.08	4.24	4.24	4.50	4.64	5.27	5.97
ϕ_3(%)	1.9±0.6	1.1±0.2									
ϕ_4	2.8±0.9	1.3±0.3	1.1±0.2								
ϕ_5	4.4±1.1	2.3±0.3	1.8±0.3	1.5±0.3	1.0±0.2	1.1±0.2	1.0±0.2				
ϕ_6	6.0±1.2	3.0±0.4	2.5±0.3	2.0±0.3	1.4±0.2	1.5±0.2	1.5±0.2				
ϕ_7	7.9±1.2	4.0±0.4	3.5±0.4	2.7±0.3	1.9±0.2	1.9±0.3	2.0±0.3	1.1±0.2	1.0±0.2		
ϕ_8	10.2±1.1	5.6±0.6	4.6±0.5	3.7±0.4	2.6±0.2	2.4±0.3	2.7±0.3	1.3±0.2	1.2±0.2		
ϕ_9	13.1±1.3	7.7±0.6	5.7±0.6	5.0±0.5	3.4±0.3	2.9±0.3	3.2±0.3	1.8±0.3	1.7±0.2	1.0±0.3	
ϕ_{10}	12.9±1.3	8.7±0.6	7.1±0.5	6.7±0.5	4.5±0.4	3.6±0.3	4.1±0.3	2.4±0.3	2.4±0.3	1.4±0.4	
ϕ_{11}	11.8±1.1	9.1±0.6	8.9±0.6	8.9±0.5	5.7±0.4	4.5±0.3	5.1±0.4	3.1±0.3	2.9±0.3	1.9±0.5	1.2±0.2
ϕ_{12}	9.5±1.1	8.2±0.6	10.0±0.7	9.9±0.5	7.0±0.5	5.9±0.4	6.4±0.4	3.8±0.3	3.7±0.3	2.3±0.5	1.6±0.2
ϕ_{13}	7.2±1.0	7.4±0.6	8.9±0.6	9.8±0.5	8.0±0.5	7.2±0.5	8.0±0.5	4.6±0.3	4.6±0.3	2.8±0.6	2.2±0.3
ϕ_{14}	5.2±0.7	6.6±0.5	7.9±0.5	8.3±0.5	8.5±0.5	7.9±0.5	8.3±0.5	5.4±0.6	5.5±0.4	3.2±0.6	2.7±0.4
ϕ_{15}	3.7±0.7	5.9±0.6	7.0±0.6	7.2±0.5	9.0±0.5	8.2±0.5	8.6±0.5	6.6±0.5	6.4±0.4	3.7±0.6	3.3±0.4
ϕ_{16}	2.0±0.4	5.1±0.5	5.8±0.6	6.1±0.5	8.1±0.5	7.4±0.5	7.8±0.5	7.5±0.5	7.1±0.4	4.2±0.5	3.9±0.5
ϕ_{17}		4.5±0.5	5.1±0.6	5.1±0.5	7.4±0.5	7.2±0.5	7.2±0.5	8.2±0.5	7.5±0.4	4.9±0.5	4.5±0.5
ϕ_{18}		3.9±0.4	4.1±0.5	4.3±0.4	6.7±0.6	6.5±0.5	6.2±0.5	8.1±0.5	7.9±0.4	5.6±0.5	5.2±0.6
ϕ_{19}		3.2±0.5	3.6±0.4	3.6±0.4	6.0±0.6	5.9±0.4	5.5±0.4	7.8±0.5	7.7±0.4	6.4±0.6	5.8±0.6
ϕ_{20}		2.6±0.4	2.9±0.4	3.0±0.4	5.1±0.5	5.2±0.4	5.0±0.4	7.1±0.5	7.2±0.4	7.1±0.6	6.5±0.7
ϕ_{21}		2.1±0.3	2.4±0.3	2.6±0.3	4.0±0.4	4.3±0.3	4.0±0.3	6.2±0.5	6.5±0.4	7.6±0.6	7.1±0.6
ϕ_{22}		1.7±0.3	2.0±0.3	2.1±0.3	3.2±0.6	3.3±0.3	3.1±0.3	5.5±0.4	5.7±0.4	7.4±0.6	7.4±0.6
ϕ_{23}		1.3±0.3	1.5±0.2	1.7±0.2	2.3±0.3	2.7±0.3	2.4±0.3	4.5±0.3	4.8±0.3	6.9±0.6	7.2±0.7
ϕ_{24}		1.0±0.2	1.0±0.2	1.3±0.2	1.6±0.3	2.1±0.3	2.0±0.3	3.7±0.3	3.9±0.3	6.2±0.6	6.8±0.7
ϕ_{25}				1.0±0.2	1.2±0.2	1.7±0.2	1.6±0.2	3.1±0.3	3.0±0.3	5.2±0.5	6.1±0.6
ϕ_{26}						1.3±0.2	1.2±0.2	2.4±0.3	2.3±0.3	4.3±0.5	5.5±0.6
ϕ_{27}						1.0±0.2	1.0±0.2	1.8±0.3	1.7±0.2	3.7±0.6	4.7±0.6
ϕ_{28}								1.2±0.2	1.3±0.2	3.2±0.6	3.9±0.5
ϕ_{29}									1.0±0.2	2.7±0.6	3.3±0.4
ϕ_{30}										2.3±0.5	2.9±0.4
ϕ_{31}										1.9±0.5	2.5±0.3
ϕ_{32}										1.5±0.4	1.9±0.3
ϕ_{33}										1.1±0.3	1.5±0.2

Table III. Some experimental and theoretical ⟨z⟩ values for "very heavy" ions.

Z_1	$v \times 10^{-8}$ (cm/sec)	⟨z⟩ (in positive electron units)			
		Gas		Solid	
		Experimental	Theoretical[a]	Experimental	Theoretical[b]
35 (Br)[c]	6.00	--	8.9	11.0	13.3
38 (Light fission fragments)[d]	11.00	13.8	16.8	19.2	25.2
54 (heavy fission fragments)[d]	6.60	10.5	11.3	17.8	17.0
	8.80	14.6	15.1	22.5	22.6
66 (Dy)	5.97	--	11.0	23.3	16.5

[a] According to Eq. (12) by Bohr.

[b] Equation (12) and factor 3/2 by Bohr and Lindhard.

[c] Reference 32.

[d] References 12, 13.

Table IV. Equilibrium ratios, ϕ_{z+1}/ϕ_z of adjacent charge-state probabilities for various velocities

	$\langle v \rangle \times 10^{-8}$ (cm/sec)										
	2.52	3.05	3.30	3.45	4.08	4.24[a]	4.24[b]	4.50	4.64	5.27	5.97
z = 5	1.36 ± 0.43	1.31 ± 0.25	1.39 ± 0.29	1.33 ± 0.33	1.40 ± 0.35						
6	1.32 ± 0.32	1.33 ± 0.20	1.40 ± 0.22	1.35 ± 0.25	1.36 ± 0.31	1.36 ± 0.31	1.50 ± 0.36				
7	1.29 ± 0.25	1.40 ± 0.20	1.31 ± 0.20	1.37 ± 0.20	1.37 ± 0.17	1.27 ± 0.25	1.33 ± 0.26				
8	1.28 ± 0.20	1.37 ± 0.20	1.24 ± 0.17	1.35 ± 0.18	1.30 ± 0.15	1.26 ± 0.25	1.35 ± 0.25	1.48 ± 0.32	1.42 ± 0.28		
9	0.98 ± 0.14	1.13 ± 0.12	1.24 ± 0.14	1.34 ± 0.16	1.32 ± 0.17	1.21 ± 0.19	1.19 ± 0.17	1.33 ± 0.28	1.41 ± 0.24	1.40 ± 0.57	
10	0.91 ± 0.12	1.05 ± 0.10	1.25 ± 0.12	1.33 ± 0.13	1.27 ± 0.14	1.24 ± 0.16	1.28 ± 0.16	1.29 ± 0.21	1.21 ± 0.18	1.36 ± 0.52	
11	0.81 ± 0.11	0.90 ± 0.09	1.12 ± 0.11	1.11 ± 0.09	1.23 ± 0.12	1.25 ± 0.14	1.28 ± 0.16	1.23 ± 0.16	1.28 ± 0.17	1.21 ± 0.36	
12	0.79 ± 0.13	0.90 ± 0.10	0.89 ± 0.08	0.99 ± 0.07	1.14 ± 0.11	1.31 ± 0.12	1.25 ± 0.13	1.21 ± 0.12	1.24 ± 0.21	1.21 ± 0.35	1.37 ± 0.25
13	0.72 ± 0.14	0.89 ± 0.10	0.89 ± 0.08	0.85 ± 0.08	1.06 ± 0.10	1.22 ± 0.12	1.25 ± 0.11	1.17 ± 0.11	1.19 ± 0.11	1.14 ± 0.30	1.23 ± 0.25
14	0.71 ± 0.15	0.89 ± 0.11	0.89 ± 0.08	0.87 ± 0.09	1.05 ± 0.10	1.10 ± 0.10	1.04 ± 0.09	1.22 ± 0.13	1.16 ± 0.10	1.17 ± 0.26	1.22 ± 0.23
15	0.54 ± 0.15	0.86 ± 0.12	0.83 ± 0.11	0.85 ± 0.09	0.90 ± 0.09	1.04 ± 0.08	1.04 ± 0.09	1.14 ± 0.12	1.11 ± 0.09	1.14 ± 0.23	1.18 ± 0.21
16		0.88 ± 0.12	0.88 ± 0.08	0.84 ± 0.11	0.91 ± 0.10	0.90 ± 0.09	0.91 ± 0.08	1.10 ± 0.11	1.06 ± 0.08	1.17 ± 0.20	1.15 ± 0.18
17		0.87 ± 0.13	0.80 ± 0.13	0.84 ± 0.12	0.91 ± 0.11	0.97 ± 0.10	0.92 ± 0.07	0.99 ± 0.08	1.05 ± 0.08	1.14 ± 0.20	1.16 ± 0.18
18		0.82 ± 0.12	0.89 ± 0.14	0.84 ± 0.12	0.90 ± 0.12	0.90 ± 0.09	0.86 ± 0.09	0.96 ± 0.08	0.97 ± 0.08	1.14 ± 0.15	1.12 ± 0.17
19		0.81 ± 0.16	0.81 ± 0.15	0.83 ± 0.14	0.85 ± 0.12	0.91 ± 0.10	0.89 ± 0.10	0.91 ± 0.09	0.94 ± 0.08	1.11 ± 0.18	1.12 ± 0.16
20		0.81 ± 0.17	0.83 ± 0.16	0.87 ± 0.15	0.78 ± 0.11	0.88 ± 0.10	0.91 ± 0.10	0.87 ± 0.10	0.90 ± 0.07	1.07 ± 0.15	1.09 ± 0.14
21		0.81 ± 0.18	0.83 ± 0.16	0.81 ± 0.14	0.82 ± 0.11	0.82 ± 0.08	0.80 ± 0.09	0.89 ± 0.10	0.88 ± 0.08	0.97 ± 0.15	1.04 ± 0.12
22		0.76 ± 0.22	0.75 ± 0.15	0.81 ± 0.15	0.72 ± 0.14	0.77 ± 0.09	0.76 ± 0.09	0.82 ± 0.08	0.84 ± 0.08	0.93 ± 0.14	0.97 ± 0.12
23		0.77 ± 0.26	0.67 ± 0.16	0.76 ± 0.14	0.70 ± 0.16	0.82 ± 0.11	0.77 ± 0.12	0.82 ± 0.08	0.81 ± 0.09	0.90 ± 0.14	0.94 ± 0.13
24				0.77 ± 0.19	0.75 ± 0.19	0.78 ± 0.14	0.83 ± 0.16	0.84 ± 0.11	0.77 ± 0.10	0.84 ± 0.13	0.90 ± 0.13
25						0.63 ± 0.09	0.80 ± 0.15	0.77 ± 0.12	0.77 ± 0.13	0.83 ± 0.12	0.90 ± 0.13
26						0.76 ± 0.14	0.75 ± 0.16	0.75 ± 0.18	0.74 ± 0.13	0.86 ± 0.17	0.77 ± 0.14
27						0.77 ± 0.19	0.83 ± 0.22	0.67 ± 0.17	0.76 ± 0.13	0.86 ± 0.18	0.83 ± 0.15
28									0.77 ± 0.19	0.84 ± 0.24	0.85 ± 0.15
29										0.85 ± 0.25	0.88 ± 0.16
30										0.83 ± 0.28	0.86 ± 0.17

[a] for reaction $Ce^{138}(O^{16},7n)Dy^{149}$

[b] for reaction $Pr^{141}(O^{16},8n)Ho^{149}$

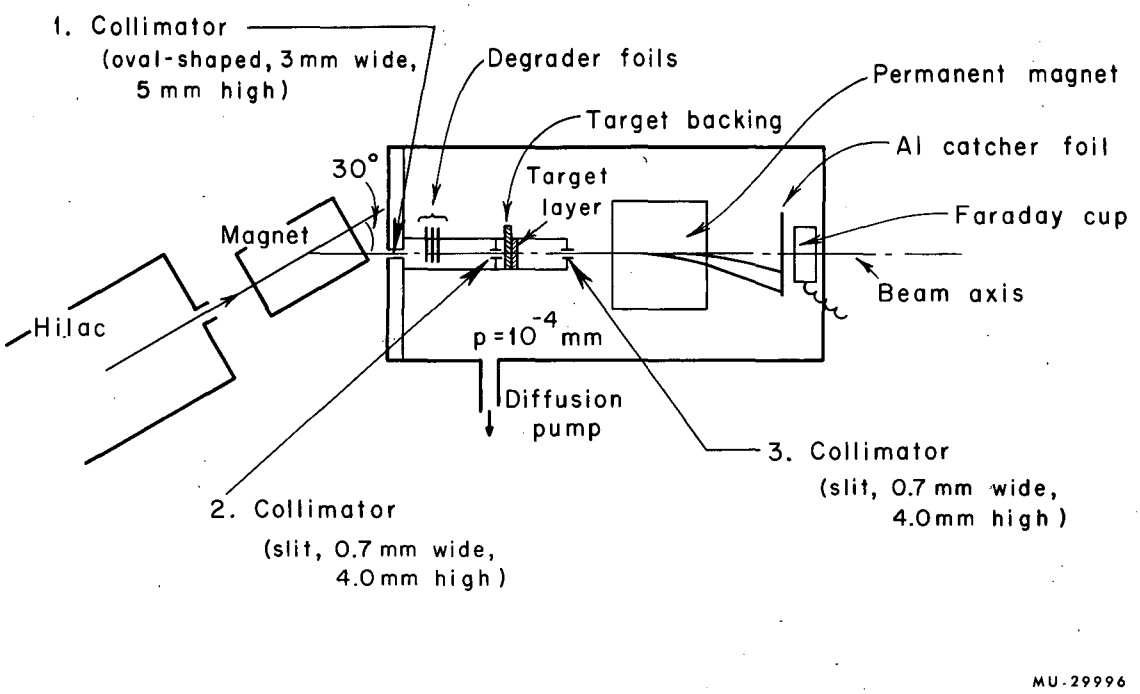

Fig. 1. Schematic diagram of experimental arrangement.

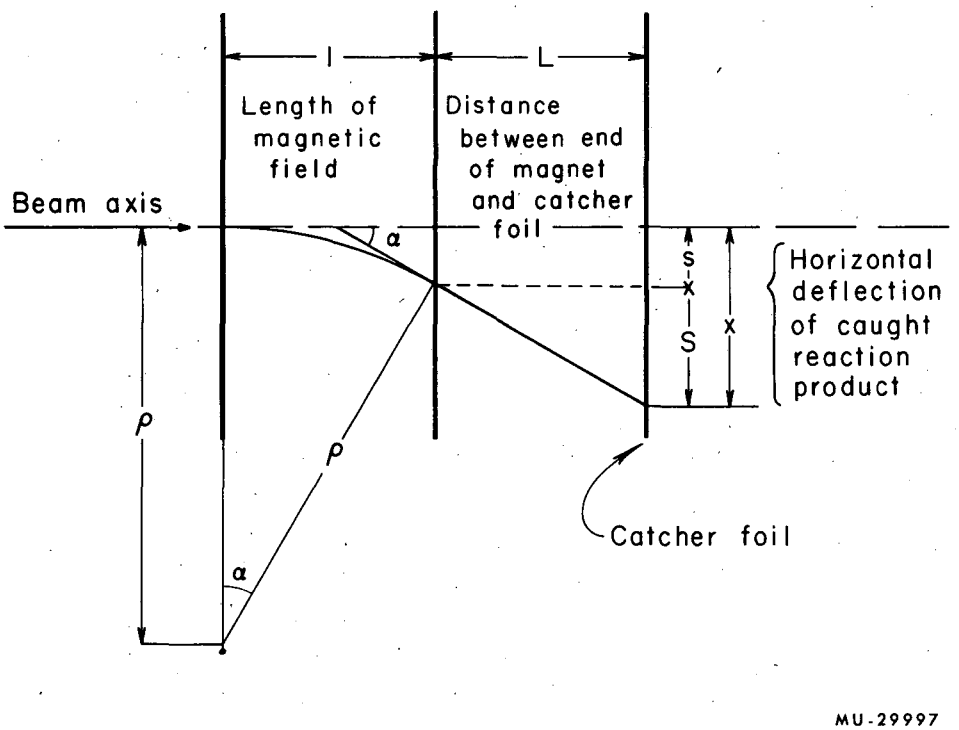

Fig. 2. Schematic representation of deflection geometry.

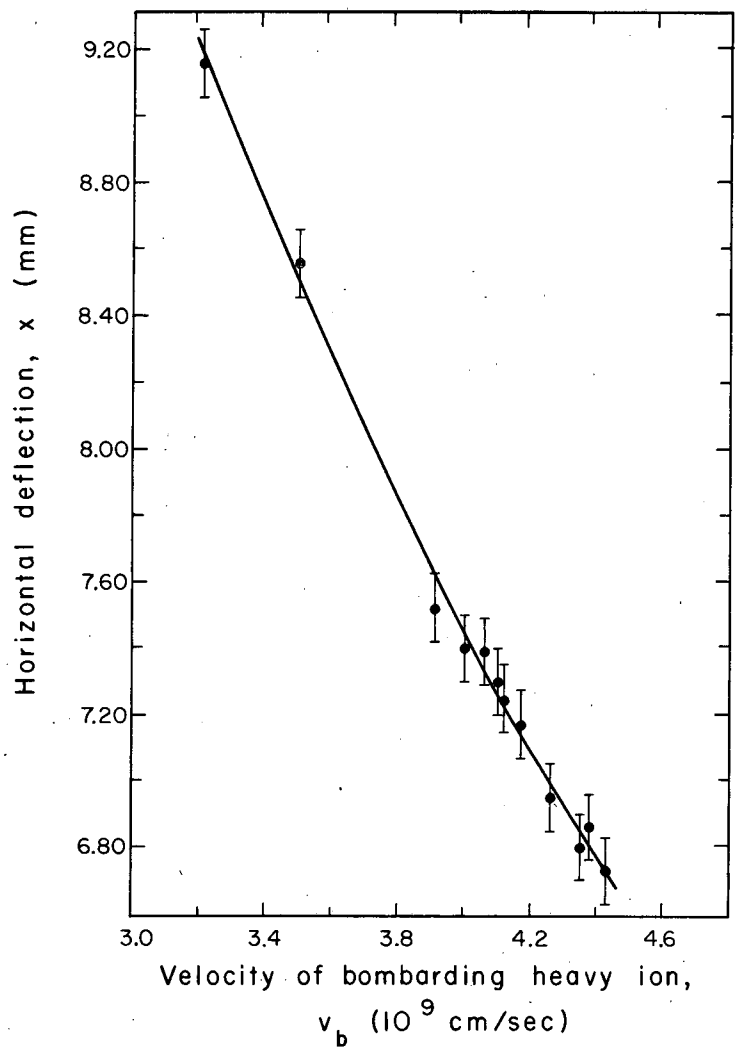

Fig. 3. Horizontal deflection of bombarding ions as a function of ion velocity, v_b:

A_1/z = 2 for all ions used (except F^{19}): C^{12}, N^{14}, O^{16}, Ne^{20}, Ne^{22}

l = 15.2 cm, L = 5.3 cm, H = 3.50 gauss.

Solid curve: according to Eq. (3)
Points: from distance measurements on catcher foils and nuclear emulsion plates (explained in text).

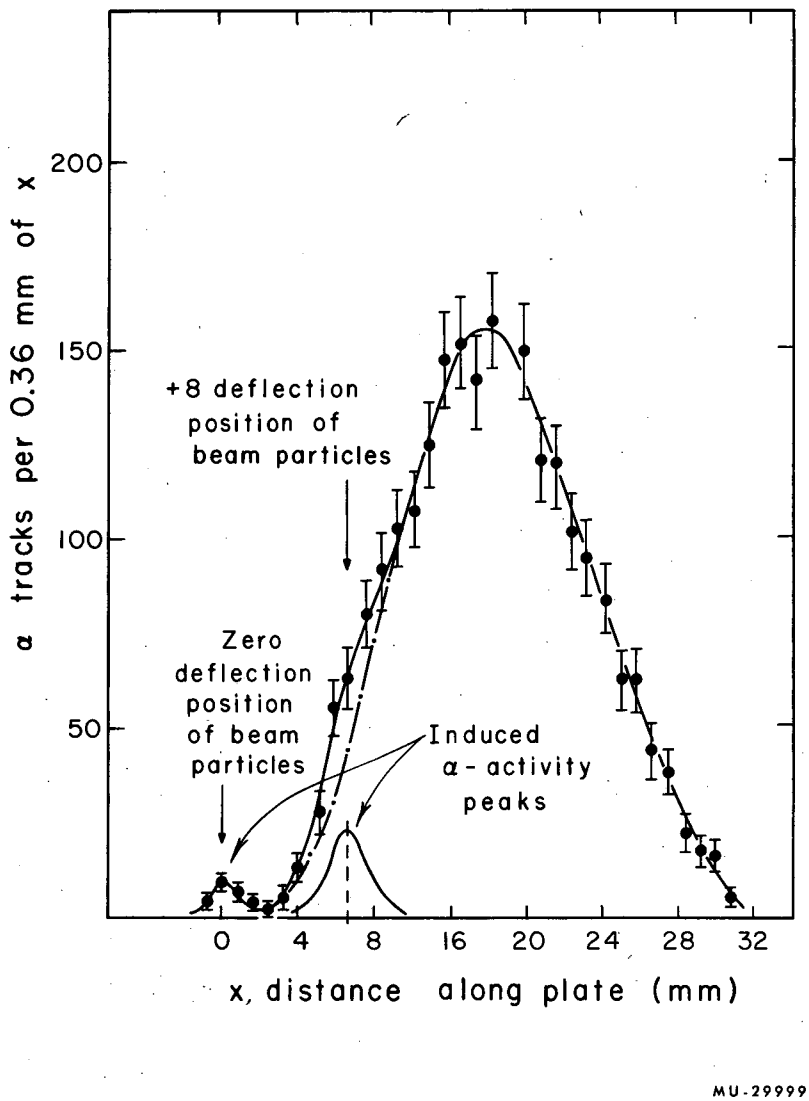

Fig. 4. Experimental scanning curve. Horizontal displacement, x, of particles on catcher foil as a function of α-particle track density.

Nuclear reaction: $Pr^{141}(O^{16},8n)Ho^{149}$.

E_b(lab) = 162.0 MeV; target thickness = 100 μg/cm^2.

Mean velocity of Ho^{149} particles: $\langle v \rangle = 4.50 \times 10^8$ cm/sec.

Magnetic field strength = 3150 gauss.

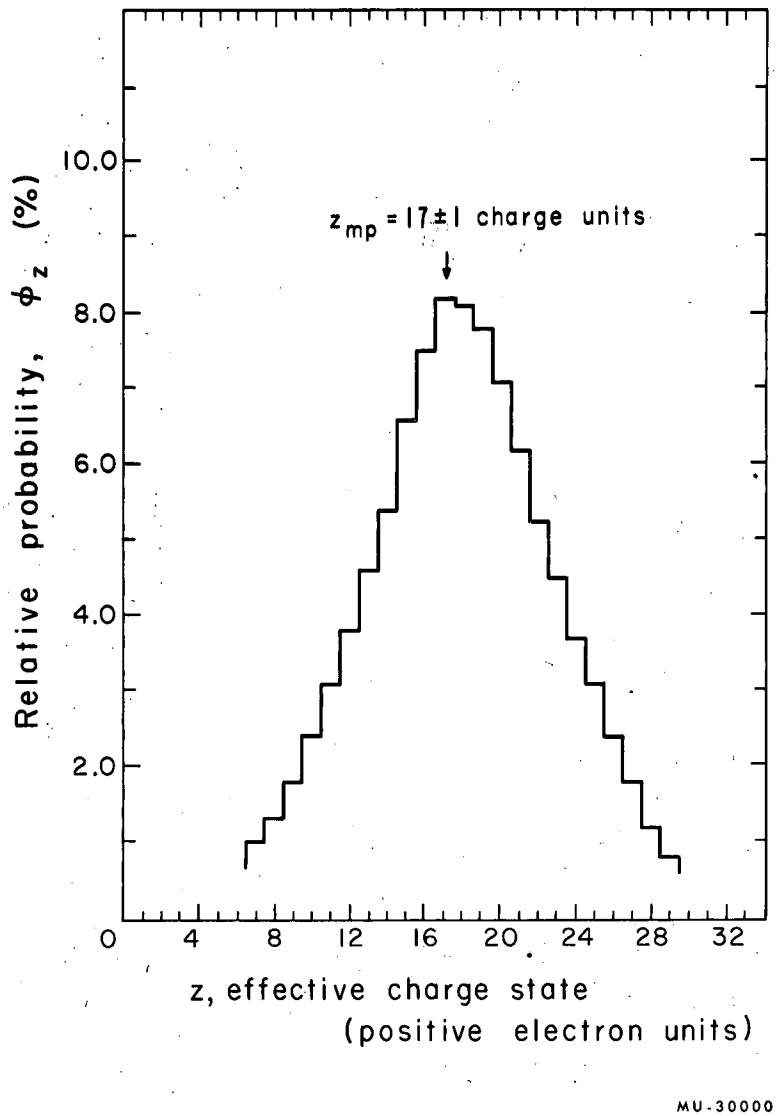

Fig. 5. Corrected charge-distribution histogram. Relative probability ϕ_z (in %) as a function of the effective charge state z (in positive electron units).

Nuclear charge of particles: $Z_1 = 67$.

Mean velocity of particles: $\langle v \rangle = 4.5 \times 10^8$ cm/sec.

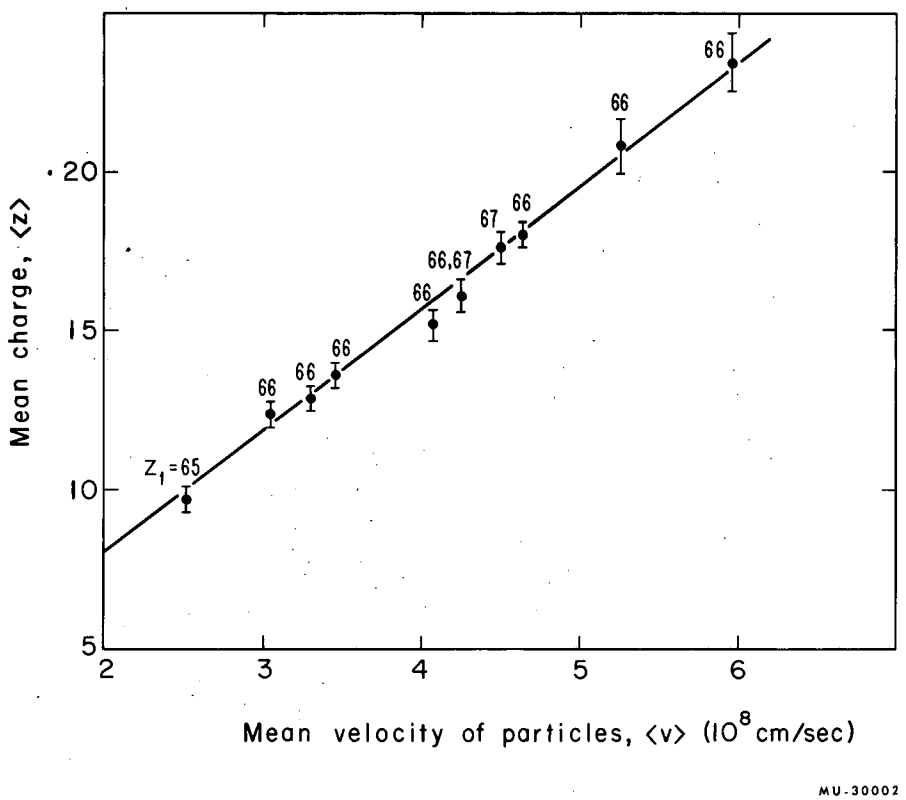

Fig. 6. Mean charge, ⟨z⟩, as a function of mean velocity of particles, ⟨v⟩. Nuclear charges of moving particles: Z_1 = 65, 66, 67.

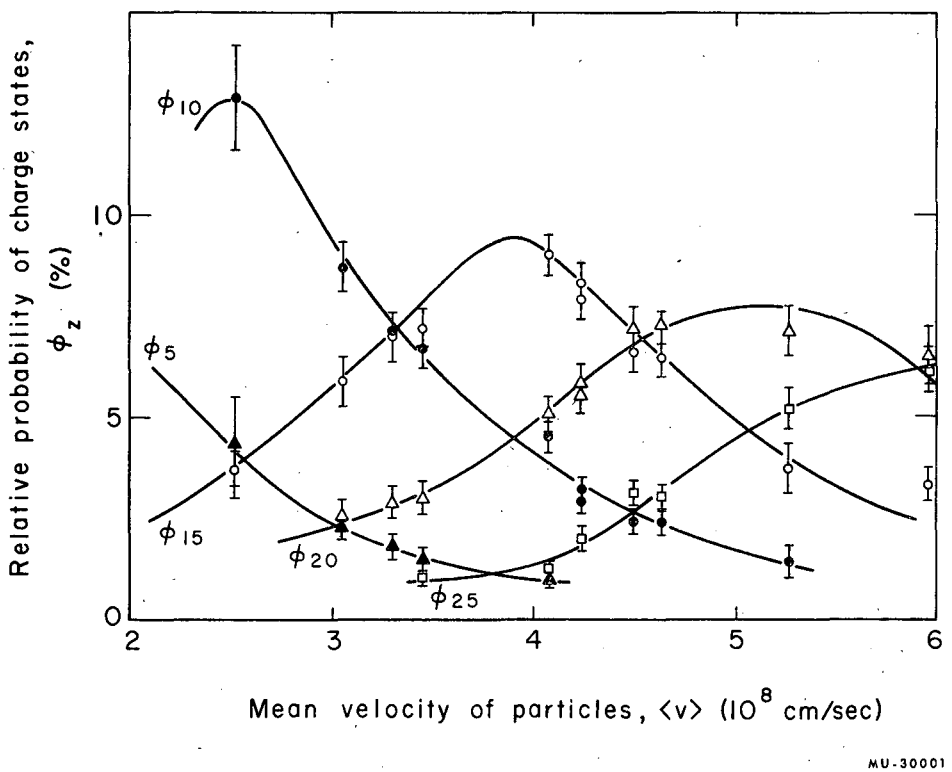

Fig. 7. Relative probabilities for some of the charge states obtained, ϕ_z (in %) as a function of the mean velocity of the particles, ⟨v⟩.

z = 5, 10, 15, 20, 25,

Z_1 = 66 ± 1
Z_2 = 56 to 60
} see Table I.

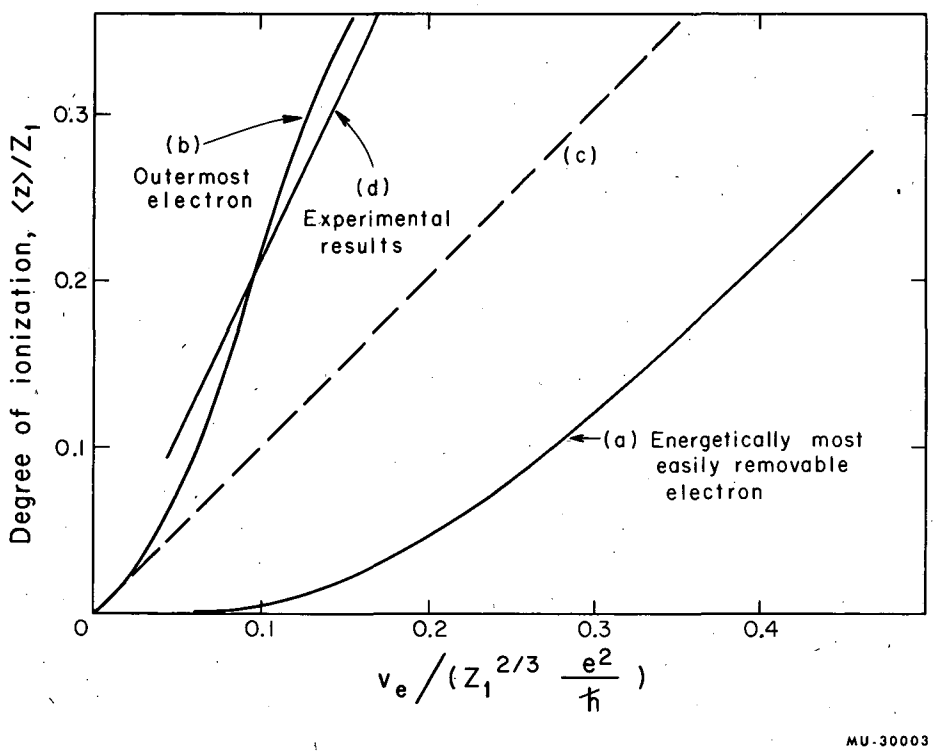

Fig. 8. Degree of ionization, $\langle z \rangle / Z_1$, as a function of the velocity characteristic of the process of electron capture and loss (see explanation in text). $Z_1 = 66 \pm 1$; $v_e = \gamma v$. Curve (c) according to Bohr (see Eq. (12)); $\bar{v}_e = v$; $\gamma = 1$.

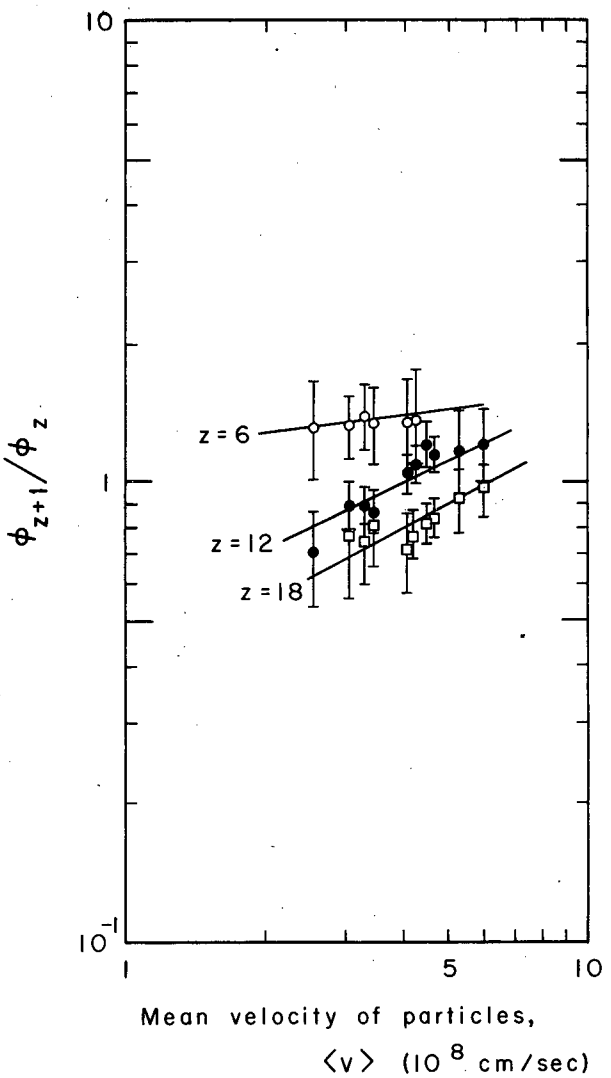

Fig. 9. Ratio of adjacent relative charge-state probabilities as a function of mean velocity of particles.
At equilibrium: $\phi_{z+1}/\phi_z = \sigma_{loss}/\sigma_{capture}$ for z = 6, 12 and 18.

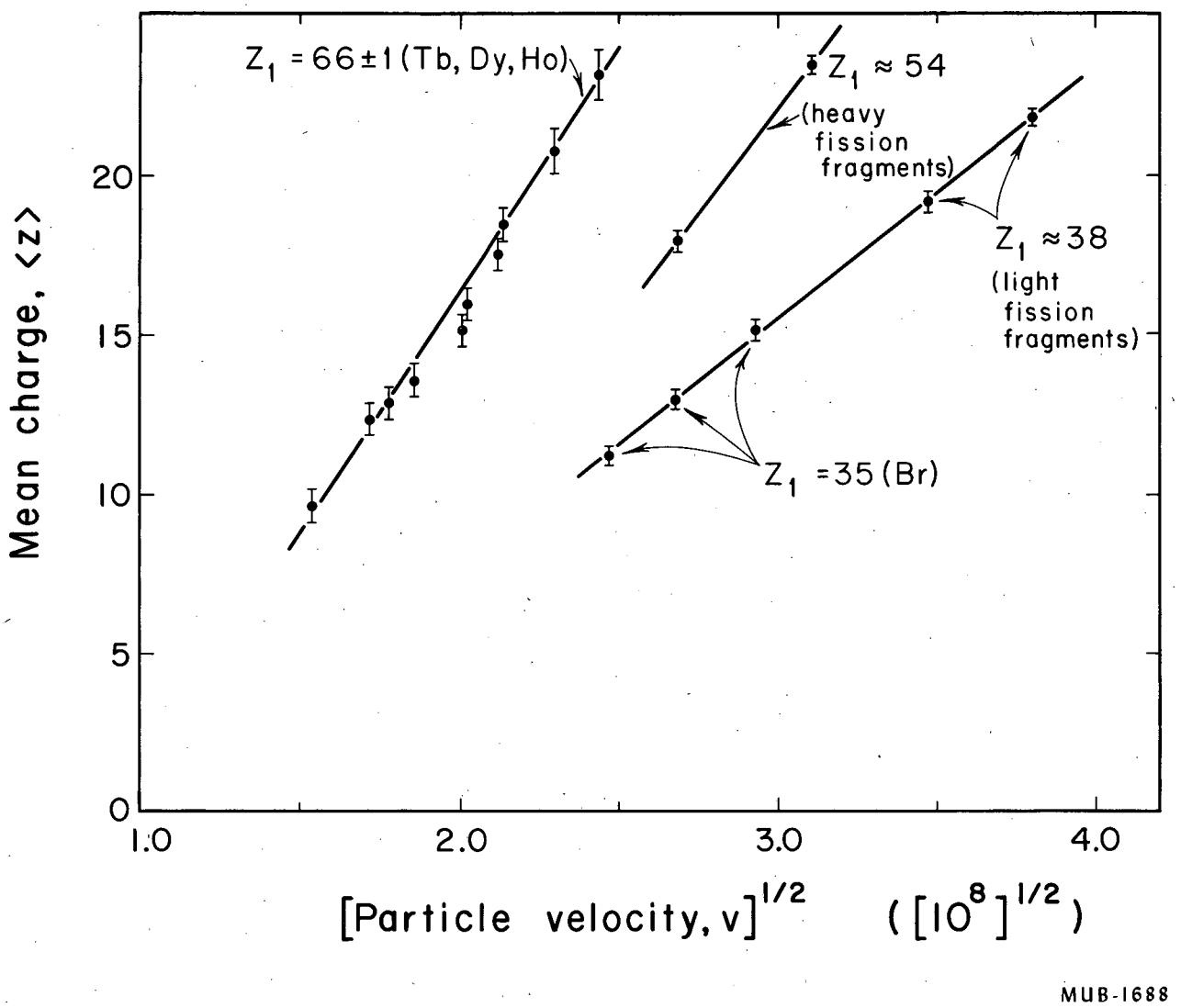

Fig. 10. Compilation of existing experimental data of the mean charge, ⟨z⟩, of "very heavy" ions as a function of the square root of the particle velocity.